THIS MANUSCRIPT IS A NON-PEER REVIEWED PREPRINT SUBMITTED TO EARTHARXIV AND IS UNDER CONSIDERATION AT VOLCANICA

SilicH$_2$O: a graphical user interface for processing silicate glass Raman spectra and quantifying H$_2$O

T. D. van Gerve [*α] and O. Namur[α]

[α] Department of Earth and Environmental sciences, KU Leuven, Belgium.

ABSTRACT

H$_2$O contents of magmas strongly impact the explosivity of volcanic eruptions, as well as their rheological properties and crystallisation behaviour. Accurate analyses of H$_2$O in magmatic liquids are therefore vital for our understanding of the dynamics of magmatic processes and eruptions. Raman spectroscopy provides an accessible, affordable and high spatial resolution technique for estimating H$_2$O contents of magmas that have been quenched to a glass during eruption. However, calculating H$_2$O concentrations from Raman spectra involves manual data processing and results are therefore sensitive to the specific treatment used. SilicH$_2$O is an open-source software program that uniformises and streamlines this process by providing an interactive graphical user-interface. It can be used to: (a) process Raman spectra of silicate glasses, (b) remove any unwanted peaks through interpolation and unmixing, (c) set up H$_2$O calibrations with reference materials and (d) quantify H$_2$O contents of unknown samples.

KEYWORDS: Raman spectroscopy; Glass; Hydrous melt; Software; Python.

1 INTRODUCTION

Knowing the H$_2$O contents of magmas is crucial for understanding their phase equilibria, crystallisation behaviour, physical properties and eventual eruption style. However, traditional methods to measure H$_2$O in volcanic glasses, such as secondary ion mass spectrometry (SIMS) and fourier transform infrared (FTIR) spectroscopy, can be expensive and require extensive sample preparation. In contrast, confocal Raman spectroscopy is affordable, requires little preparation and has similarly high spatial resolution, but requires (often) complicated post-processing of collected spectra. The most important processing step is removal of background signal, for which different authors use different algorithms, producing different results. Moreover, the tools used for processing are not always made publicly available and the ones that are typically rely on code (e.g. `Python`, `Matlab`) that users have to implement themselves (e.g. Le Losq et al. 2012; Di Genova et al. 2017). SilicH$_2$O is an open-source software program that streamlines and uniformises post-processing of Raman spectra by providing an intuitive graphical user interface (Figure 1). It is aimed at quantifying H$_2$O in silicate glasses of any composition and integrates tools for unwanted peak removal, background subtraction and H$_2$O calibration. Results produced with SilicH$_2$O indicate that with the implemented data processing algorithms H$_2$O can be measured by Raman spectroscopy with accuracies and precisions of mostly below 0.1 wt.%.

This manuscript introduces the main concepts of silicate glass Raman spectroscopy and its H$_2$O calibration and reviews the most important features of SilicH$_2$O (version 1.0.0). The software is available for Mac and Windows and can be downloaded from GitHub[†], with step by step installation and usage instructions available in its documentation[‡].

2 RAMAN SPECTROSCOPY

Raman spectroscopy is based on the analysis of inelastically scattered light inside solids, liquids and gasses (Raman 1928; Frezzotti et al. 2012; Pasteris and Beyssac 2020). In a Raman spectroscope, a monochromatic laser is focused on a sample, exciting the vibrations of molecular bonds within the sample. This transfer of energy between the incoming laser's photons and molecular vibrations inelastically scatters the outcoming photons causing shifts in their vibration frequency and these shifts are then measured in wavenumer units (cm^{-1}). Raman shifted frequencies depend on molecular composition and vibrational mode (stretching or bending), while the scattered light intensity is (amongst other things; e.g. acquisition parameters) proportional to concentration of chemical species (Neuville et al. 2014; Malfait 2018). As such, Raman spectra of scattered light intensities as a function of their frequencies offer qualitative information on both the structure and composition of analysed samples.

---

[*] ✉ thomas.vangerve@kuleuven.be

[†] https://github.com/TDGerve/silicH2O

[‡] https://silich2o.readthedocs.io/en/latest/

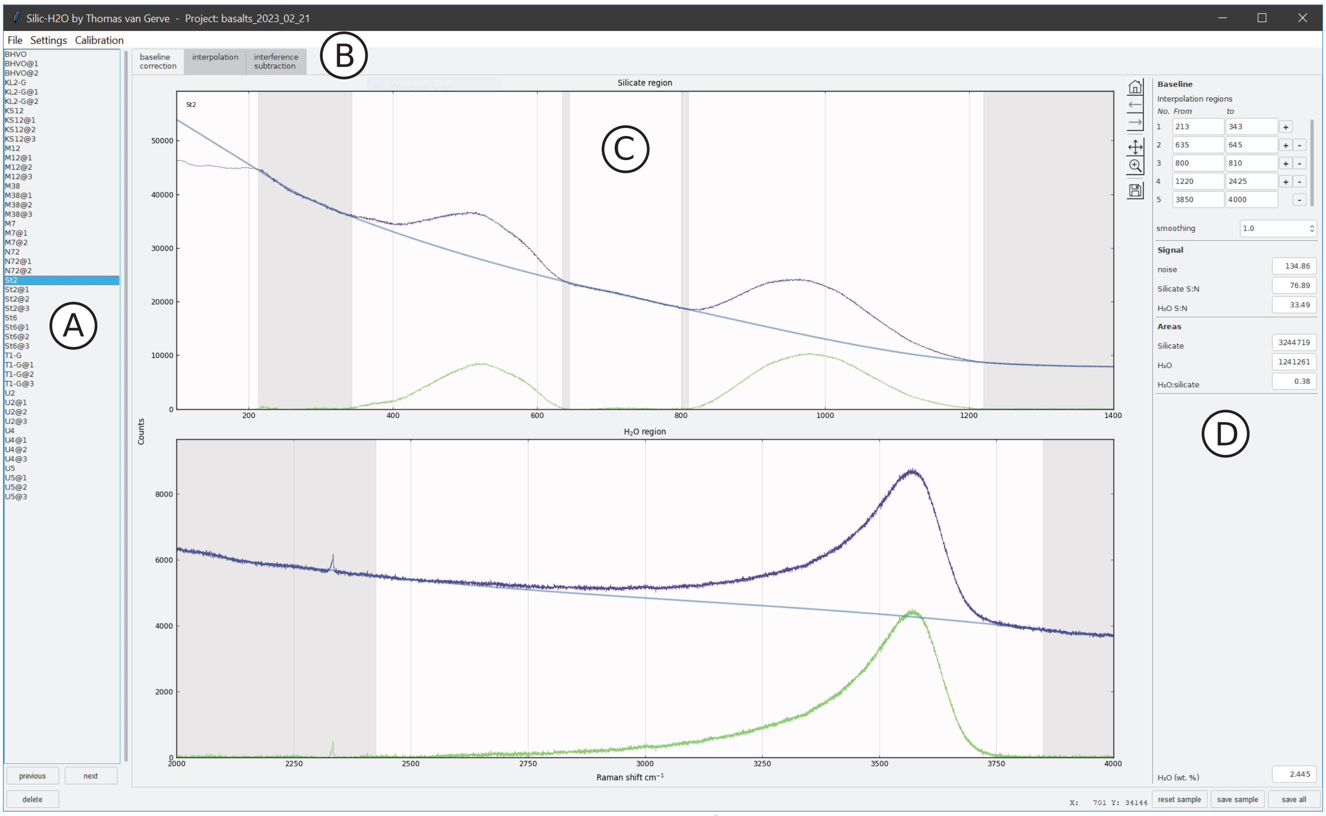

Baseline

Interpolation regions

No.	From	to
1	213	343
2	635	645
3	800	810
4	1220	2425
5	3850	4000

smoothing: 1.0

Signal

noise: 134.86
Silicate S:N: 76.89
H₂O S:N: 33.49

Areas

Silicate: 3244719
H₂O: 1241261
H₂O:silicate: 0.38

H₂O (wt. %): 2.445

Figure 1: The main user interface of `SilicH`$_2$`O` (running on Windows OS), with **A** sample selection bar, **B** tool selection bar, **C** interactive spectrum with baseline interpolation regions as grey bars and **D** settings and results bar.

2.1 Analytical considerations

The focus of this paper is on measuring H_2O in glasses. Some care has to be taken during analyses, as glasses heat up due to partial absorption of the laser light. In opaque glasses, such as glasses with high iron contents or nanoscale crystals, this may lead to water loss or even melting (Behrens et al. 2006; Thomas et al. 2008). Optical properties vary from glass to glass and sensitivity to the laser should be tested for each sample before analysis by gradually increasing laser power and checking for potential burn marks (Supplementary Figure S1). If samples are embedded in or otherwise held in place by glue or resin it is also important to make sure that they are not fluorescent or Raman active at frequencies within the desired spectral range.

2.2 H_2O quantification

H_2O dissolved in silicate glass produces Raman signal between 2200 and 4000 cm^{-1} (Figure 2 and 3B) and analysis of the intensity of this H_2O band is the basis for all existing H_2O calibrations. There are two general calibration methods: external and internal. The external method quantifies the relationship between the integrated area (or sometimes height) of Raman H_2O peaks (I_{H_2O}) and glass H_2O contents by regressing known H_2O contents of calibration materials against their measured I_{H_2O} (Behrens et al. 2006; Mercier et al. 2009; Schiavi et al. 2018). The internal method first normalises I_{H_2O} to the integrated area of one or more Raman peaks in the silicate region (I_{Si}) of the analysed sample (Zajacz et al. 2005; Le Losq et al. 2012; Di Genova et al. 2017) and then compares this ratio (I_{H_2O}/I_{Si}) to known H_2O contents in calibration materials. This method increases reproducibility and reduces the effects analytical conditions and instrumental setup (laser power, counting time, etc.) have on the calibration. Additionally, some authors (e.g. Le Losq et al. 2012; Di Genova et al. 2017; Schiavi et al. 2018) correct raw intensities for frequency and temperature dependencies (the Long correction Long 1977; Neuville and Mysen 1996)

2.3 Spectral processing

Since Raman spectra include fluorescent background signal (Figure 2), peak height and area cannot be calculated directly from raw spectra and first require a baseline fitting strategy. This baseline is fitted to areas of the spectrum without peaks (baseline interpolation regions, *BIRs*) and subsequently extended to the entire spectrum. Various algorithms have been used in the past including linear extrapolation (Zajacz et al. 2005) and interpolations with polynomials (Thomas et al. 2008), cubic splines (Behrens et al. 2006; Di Genova et al. 2017) or smoothing splines (Le Losq et al. 2012). While different algorithms give baselines with different local curvatures, the overall shape is mostly controlled by *BIR* placement (e.g. Di Muro et al. 2009). Where and how many of these should be placed depends on the peak positions and shapes and determining this in a consistent way requires prior knowledge on the parameters that influence spectrum topology. Still, the fact that different procedures have been proposed in recent publications shows that this remains subject to interpretation and is not a straightforward exercise (cf. Le Losq et al. 2012; Di Genova et al. 2017; Schiavi et al. 2018). Another aspect that has to be taken into account is that Raman instrumental setup may also influence *BIR* placement. For instance, gratings with narrower groove spacings have higher spectral resolutions and produce narrower peaks than coarser gratings (e.g. 1800 vs. 150 grooves/mm.), affecting spectrum topologies. Lastly, since background shapes and intensities may even vary within single glasses (Section 4.2), it is important to process and inspect spectra individually.

2.4 Silicate glass spectrum topology

The alumino-silicate network of glasses produces Raman peaks in the region 200–1300 cm^{-1}, where the topology is controlled by the structure and composition of the glass (Figure 2; McMillan and Piriou 1982; Schiavi et al. 2018; Giordano et al. 2020). This region is characterised by two main bands between 200–660 cm^{-1} (Figure 3A, low wavenumbers; LW) and 800—1300 cm^{-1} (high wavenumbers; HW), with a minor band often separating the two (medium wavenumbers; MW).

2.4.1 *LW band*

In the silicate network, vibrations of bridging oxygen (BO) part of tetrahedral rings produce peaks with positions between 400 and 660 cm^{-1} (Sharma et al. 1981; McMillan et al. 1994; Neuville et al. 2014). The more tetrahedra are part of these rings, the lower the wavenumber of the produced peak. In pure SiO_2, BO vibrations in rings with three, four and five or more tetrahedra produce peaks at respectively 660, 485–490 and 440 cm^{-1} (Sharma et al. 1981; Umari et al. 2003). In practice this means that as glasses get more polymerised and the silicate network expands, the envelope of the LW band shifts to lower wavenumbers and its overall intensity increases (Di Genova et al. 2015).

2.4.2 *HW band*

The HW band is made up of a mixture of peaks resulting from stretching of T-O- bonds, where T is a tetrahedral, network forming cation (mainly Si^{4+}, Al^{3+} , Ti^{4+} or Fe^{3+}) and O- non-bridging oxygen (NBO, McMillan 1984; Mysen 2003). These stretching units are referred to as Q^n units, where n is the amount of BO and $4 - n$ the amount of NBO the cation is bonded with, meaning a Q^4 unit is fully polymerised. While peak positions also depend on the cation involved (Mercier et al. 2009), they increase to higher wavenumbers as the Q species increase from Q^1 to Q^4 (Neuville et al. 2014). Contrastingly, as molar proportions of depolymerising, network modifying elements like alkalis or alkaline-earths increase, positions of peaks for all Q species shift to lower wavenumbers and their intensities increase (Neuville et al. 2014). The overall result is that the HW envelope of more silica rich, polymerised glasses shifts towards higher wavenumbers (Di Genova et al. 2015).

2.4.3 *MW band*

The MW band is relatively weak in intensity and commonly attributed to Si-O stretching, where peak heights correlate with glass silica content (Ardia et al. 2014; Neuville et al. 2014, and references therein).

2.4.4 *H_2O region*

O-H stretching in OH groups and molecular H_2O produces a broad peak between 2200 and 4000 cm^{-1} (Figure 2 and 3B; Mysen and Virgo 1980; Malfait 2018). This peak is itself a convolution of multiple peaks produced by OH groups with different geometries and as a result has an overall asymmetric shape, where its height and width are proportional to H concentration (Behrens et al. 2006; Le Losq et al. 2012; Schiavi et al. 2018).

2.4.5 *Volcanic glasses*

For volcanic glasses, the combined behaviour of the LW, HW and MW bands means that as melts change in composition from basaltic to rhyolitic compositions, the topology of their Raman spectra undergoes distinct changes (Di Genova et al. 2015; Giordano and Russell 2018). A useful parameter to describe the structural and chemical properties of these melts is NBO/T (NBO divided by the total sum of tetrahedral cations; Mysen 1983), where low values indicate high degrees of polymerisation and high silica contents and vice versa. In basaltic glasses with high NBO/T values the HW band is located at relatively low wavenumbers with high intensities, whereas the LW band is located at relatively high wavenumbers with lower intensities. As NBO/T decreases towards more rhyolitic compositions, the HW band shifts to higher wavenumbers and lower intensites, while the LW band increases in intensity and shifts to lower wavenumbers and the MW band becomes more pronounced (Figure 3A). The overall result is that as glasses get compositionally more evolved, the distance be-

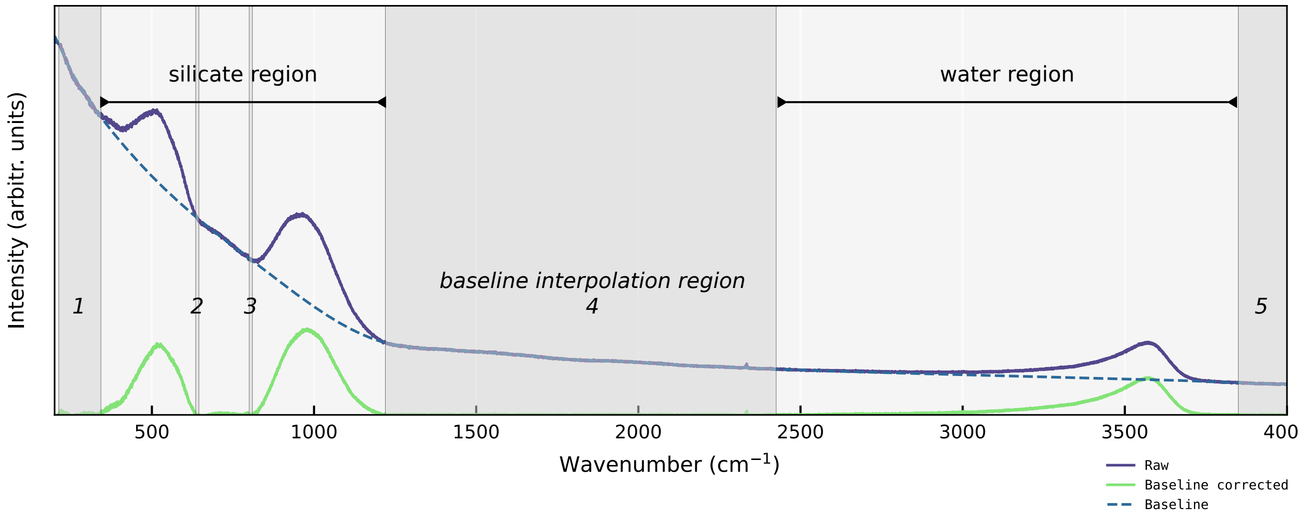

Figure 2: Baseline corrected Raman spectrum of a hydrous silcate glass. The baseline is calculated with five baseline interpolation regions (dark gray bands)

tween the LW and HW band increases. Additionally, with melt compositional evolution the intensities of the LW and HW bands increase and decrease respectively (i.e. LW/HW increases) and Giordano et al. 2020 found that at NBO/T values below 0.2—0.4 the highest intensity band changes from the HW to the LW band.

3 SPECTRUM PROCESSING WITH SilicH$_2$O

`SilicH₂O` provides a graphical user interface with all tools necessary for quantifying H_2O in silicate glasses (Figure 1). The implemented algorithms are flexible and allow for different approaches to baseline correction and calibration. Importantly, all parameter settings can be changed interactively and results are shown in real-time. This allows for fast and easy quality control and improves reproducibility compared to command line coding tools. For many calculations, code from the `Python` library `ramCOH` (version 1.1.1) is used and users are referred to its documentation (ramcoh.readthedocs.io) for a comprehensive description of the implemented algorithms. If preferred `ramCOH` can also be used without the `silicH₂O` interface as a Python command line and scripting tool. Note that `SilicH₂O` is a standalone program, does not require previous installation of `Python` or any other dependency and is compatible with `Mac` and `Windows` operating systems.

3.1 File associations

Spectra are imported from text files with columns for wavenumbers and signal intensities. When data are saved, they are stored together with their calculation settings and results in project files with a `.h2o`. Project files can hold any number of spectra and can be exchanged and shared between users, encouraging transparent and reproducible data processing. Processed spectra, results (e.g. integrated peak areas, H_2O contents) and settings (e.g. *BIR* positions) can be exported as tables in `.csv` format for further analyses or plotting. Alternatively, plots can be saved as is, directly from the interface. Any projects can be used to calculate calibration curves, as long as sample H_2O contents are known. Calibrations are saved individually in `.cH2O` files and they can be assigned to any project.

3.2 Tools

From the tool bar three main processing options can be selected (Figure 1B): baseline correction (Section *3.2.1*), interpolation (Section *3.2.2*) and interference subtraction (Section *3.2.3*). Interpolation and interference subtraction provide tools for removing unwanted peaks from the glass signal and are optional processing steps, whereas baseline corrections will always be calculated.

3.2.1 *Baseline correction*

Baselines are calculated by interpolating smoothing cubic splines between *BIRs*. A minimum of three is needed over the entire spectrum, but otherwise the user is free to add or remove *BIRs*. *BIR* location and width are changed by clicking and dragging in the main plot (Figure 1C) or by setting exact boundary values in the settings bar (Figure 1D). Alternatively, they can be copied and pasted between samples, allowing for quick and easy comparison. Smoothness of the baseline is adjusted with the *smoothing* parameter in the settings menu, which gives linear baselines as it approaches 0, while at higher values (»1) the raw data will be followed more closely. By giving the flexibility to adjust *BIR* location and amount, as well as baseline smoothness, the user is

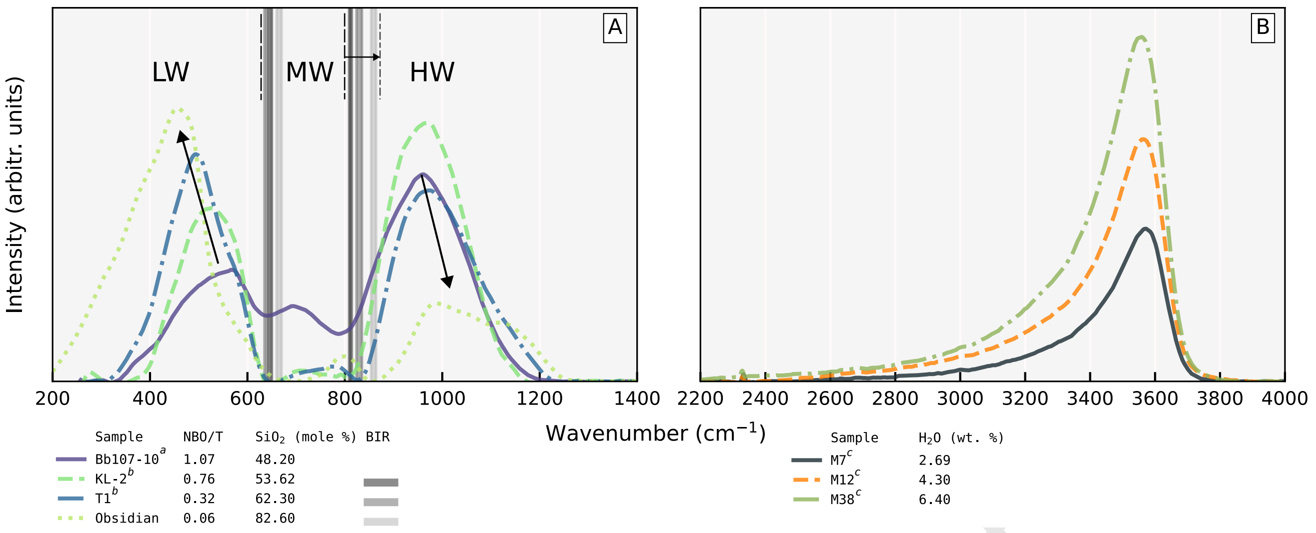

Figure 3: **A** The Raman silicate region of glasses with varying NBO/T (calculated according to Mysen and Virgo 1980). As NBO/T decreases the low wavenumber band (LW) increases in intensity and shifts to lower wavenumbers, while the high wavenumber band (HW) decreases in intensities and shifts to higher wavenumbers (arrows, Section *2.4.5*) - suggested *BIR* positions shift accordingly. Note that sample Bb107-10 has no intermediate *BIRs* as the LW and HW peaks are close enough together that they overlap and signal in the MW region does not reach the baseline. **B** The Raman H_2O region of hydrous silicate glasses with varying H_2O contents. As H_2O increases, peak intensity and width increase (Section *2.4.4*). ^{a}Médard and Grove 2008, ^{b}Jochum et al. 2006, ^{c}Shishkina et al. 2010

free to implement any of the existing baseline fitting strategies (Section 2.2). Note that baseline corrections are applied to raw spectra; the Long correction (Section 2.2) is currently not implemented as we found that it did not improve results. If needed, Long corrections can still be applied to processed spectra exported from `SilicH`$_2$`O` and `ramCOH` (Section 3) implements a method in `Python` to do so.

Integrated peak areas of the silicate and H_2O regions and their ratio are recalculated with each parameter change and displayed in the results bar (Figure 1D). The results bar also shows average spectrum noise, which is calculated as two standard deviations on the baseline corrected signal in areas without peaks (i.e. the *BIRs* set by the user). Some care has to be taken to make sure that *BIRs* only contain baseline signal, as noise values are only realistic if these regions indeed contain no peaks. Signal-to-noise ratios are then calculated for the silicate and H_2O regions each as *maximum local intensity/noise*. H_2O region signal-to-noise can be used to optimise analytical settings; if this value is below two (i.e. when signal starts to approach the noise level), counting time or laser power should perhaps be increased to get more signal, while at high ratios counting time could be reduced for more efficient time use. If a calibration file is linked with the active project (Section *3.2.4*) H_2O concentration is also recalculated with each parameter change and displayed in the results bar.

3.2.2 *Interpolation*

Unwanted peaks may appear in glass spectra due to nanocrystalline impurities (e.g. Di Genova et al. 2017) or interference from nearby phases (e.g. resin; Figure 4A Behrens et al. 2006). If these peaks overlap with the silicate or H_2O regions they will affect calculated glass H_2O contents and it is therefore best to remove them. The most straightforward way to do this is to replace the regions with unwanted peaks by interpolations calculated from the rest of the spectrum (Figure 4A). `SilicH`$_2$`O` allows the user to set one or multiple target regions for interpolation by clicking and dragging in an interactive plot. The interpolation algorithm is the same as in the baseline correction tool (Section *3.2.1*) and its parameters are set in the same way. Interpolations are shown in real-time as the user adjusts these parameters to best match the results with their estimate of the unaffected signal. Note that interpolation should only be applied when the unwanted peaks are clearly defined and when interpreting the original unaffected signal is straightforward. For spectra with with strong interference the unmixing tool is potentially a better suited option (Section *3.2.3*).

3.2.3 *Interference subtraction*

Signal interference from nearby crystalline phases is common in analyses of crystal hosted melt inclusions (Section 4.1) and may also occur in glass spectra from crystalline experimental charges or glass-dominated volcanic rocks. However, in such cases the interfering phase can also be analysed seper-

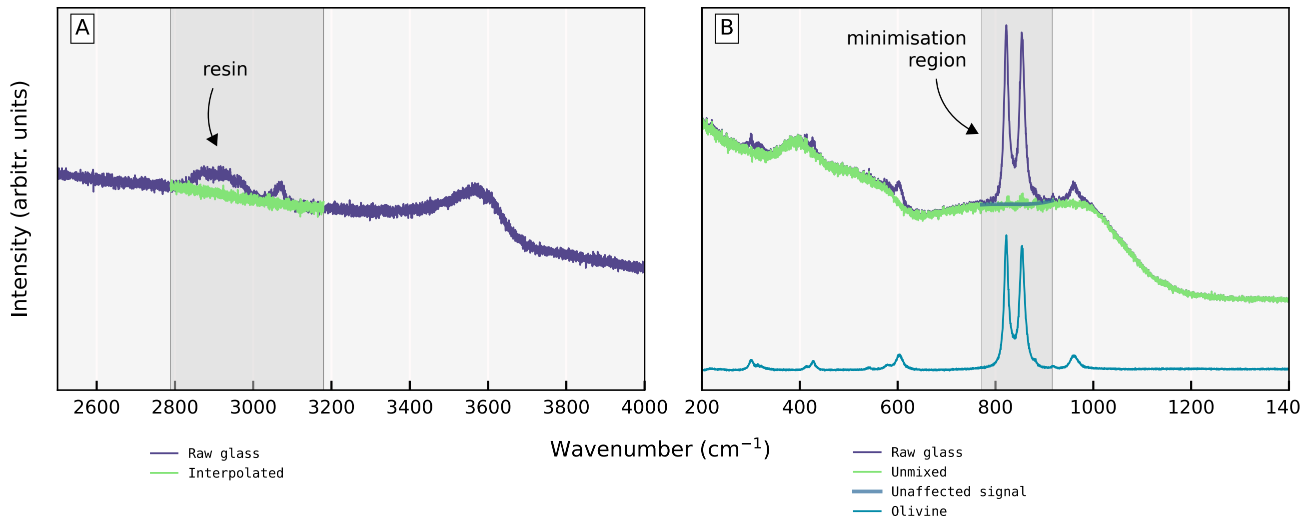

Figure 4: **A** Silicate glass spectrum with unwanted peaks from epoxy resin removed by interpolation (sample PI65-04-03 from van Gerve et al. 2023). **B** Spectrum of a glassy olivine hosted melt inclusion with interfering peaks from the olivine host removed by unmixing and interpolation (sample PI052-03-02 from van Gerve et al. 2023).

ately and this makes it possible to numerically unmix the glass and interference signal (Figure 4B).

In `SilicH`$_2$`O` unmixed signal is calculated by subtracting baseline corrected inferference signal from the raw, mixed glass signal. Scaling of the interference is numerically optimised by minimising the difference (as root-mean-square error, RMSE) between the unmixed spectrum and a calculated unaffected signal within a region set by the user. Unaffected signal is calculated from a cubic spline interpolation across the minimisation region, which should be narrow and ideally contain the highest interfering peak(s) (Figure 4B). The areas directly left and right adjacent should be free from interference, since these areas strongly impact how unaffected signal is calculated and additional interference peaks present here would give unrealistic results. Finally, the scaled interference is subtracted from the entire spectrum, removing all associated unwanted peaks.

To illustrate: olivine has two main overlapping Raman peaks between 800 and 900 cm^{-1}, as well as few minor ones (Figure 4B). With such a spectrum the best minimisation region would be one that closely brackets only the major peaks. If there are small discrepancies between peak shapes in the mixed glass signal and the interference itself, large peaks may still leave behind minor unwanted signal. In such cases interpolation (Section *3.2.2*) can be used for additional correction.

Access to these functionalities is provided in the *interference correction* tab of the tool selection bar (Figure 1B). Here, the user first links interference spectra to their corresponding glass spectra by importing them from text files. Baseline corrections of the interference are then set interactively, identical to the procedure for glass spectra (Section *3.2.1*). Users have the option to deconvolve the baseline corrected interference before unmixing, which has the added benefit that deconvolutions are noise-free. However, the user should visually compare the deconvoluted and baseline corrected signals and make sure they have a good fit. Further details on deconvolution parameters and settings can be found in the `SilicH`$_2$`O` quickstart guide and the `ramCOH` code documentation. Lastly, the location and width of the minimisation region is changed by clicking and dragging it in an interactive plot, where the calculated unaffected spectrum is also displayed and updated in real-time.

3.2.4 *Calibration*

In the calibration menu active projects can be imported and used to calculate calibration curves. The users assigns known H_2O concentrations to each sample and selects which samples should be included in the calibration. Currently, `SilicH`$_2$`O` only supports internal calibration (Section 2.2). However, it is still possible to use results exported from `SilicH`$_2$`O` for external calibration, but this has to be done manually with other software or code (e.g `Excel`, `Python`, `R`). With the internal calibration, linear regressions are calculated in `SilicH`$_2$`O` as:

$$H_2O = a + b \times \frac{Area_{H_2O}}{Area_{Silicate}} \tag{1}$$

Since the calibration curve is linear, only a limited number of calibration materials is needed in theory, but they should at least cover the full range of expected H_2O contents in the samples to be measured. R^2, standard estimate of error (SEE) and p-value regression statistics are provided and updated as samples are added or removed from the calibration. In addition to regression statistics, the fitted value for the intercept (a, Equation 1) can be used as a quality check, as this should be approximately zero. Calibration files are saved with `.cH2O` extensions and these files can be linked to any project and shared between users. However, it should be kept in mind that calibration curve slopes (b, Equation 1) are specific to each Raman instrument and calibrations should only be applied to spectra obtained with the same instrument. Additionally, calibration curves have different slopes with different spectral resolutions and if gratings with different groove spacings are available on a single Raman instrument, a separate calibration is needed for each grating.

4 REPRODUCIBILITY

Accuracy and precision of results produced with SilicH$_2$O were tested with a validation dataset of 145 glasses. It contains experiments on basalts and their residual liquids from from Médard and Grove 2008 and Neave et al. 2019 and Azorean basaltic olivine hosted melt inclusions (MI) from van Gerve et al. 2023, under review. They have 45–58 wt.% SiO_2, NBO/T of 0.42–1.09 wt.% and 0–4.4 wt.% H_2O (see Supplementary Figures S1 and S2). For calibration, a set of 13 experimental glasses with 47–58 wt.% SiO_2, 0.33–0.84 NBO/T and 0–6.4 wt.% H_2O was used. All hydrous calibration glasses are from Shishkina et al. 2010, with additional dry ones from Jochum et al. 2006 and Duggen et al. 2007. Raman analsyses were done at the Department for Earth and Environmental Sciences (KU Leuven), with specifics on instrumental setup, analytical settings and calibration detailed the Supplementary Text. Spectra of all validation samples are provided in the example projects bundled with SilicH$_2$O

4.1 Accuracy

Raman results are generally within 0.2 wt.% of reference values, with RMSE values on the validation of 0.05–0.08 wt.% (Figure 5 and Supplementary Data). Still, these values are relative to references values (from SIMS and FTIR) and absolute accuracies also depend on their respective accuracies. Validation errors (ΔH_2O, $Raman - reference$ H_2O) are normally distributed and show no systematic under- or overestimations. Additionally, ΔH_2O is consistent across varying H_2O contents and glass compositions.

A subset of the olivine hosted melt inclusions showed interference peaks from the crystal host in their Raman spectra (e.g. Figure 4B). However, after unmixing their spectra with the interference correction and interpolation tools in SilicH$_2$O, validation errors were identical to those in samples free from interference [Azores MI (unmixed), Figure 5]. This shows that with careful data treatment, even samples with unwanted peaks can be used to accurately determine H_2O contents.

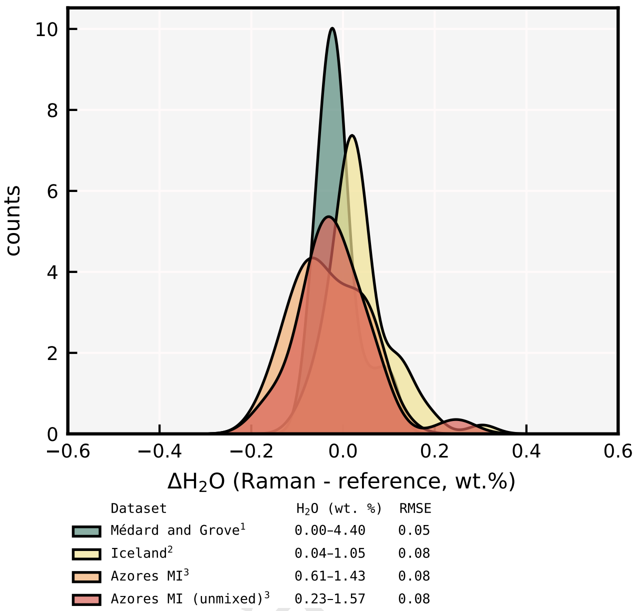

Figure 5: Reference and measured H_2O in validation datasets with basaltic glasses from [1]Médard and Grove 2008, [2]Neave et al. 2019 and [3]van Gerve et al. 2023, under review. For the Azores melt inclusions part of the data were corrected for interfering host olivine peaks by unmixing (Section *3.2.3*)

sample	**H_2O ref.**	**H_2O SNR**	**mean H_2O**	**1σ**	***n***
N72[a]	0.32	3.0	0.31	0.03	12
M7[b]	2.69	17.9	2.64	0.09	9
M12[b]	3.95	26.3	3.91	0.08	17
M38[b]	6.4	39.3	6.36	0.06	14

Table 1: 1σ precisions and signal-to-noise ratios for glasses with various reference H_2O contents (wt. %). [a]Duggen et al. 2007, [b]Shishkina et al. 2010

4.2 Precision

Analytical precisions were calculated from repeat analyses of a subselection of the calibration materials as one standard deviation (1σ) on their calculated H_2O contents. For all samples precision was below 0.1 wt. %, with no apparent relation with neither H_2O content nor H_2O signal-to-noise ratio (SNR, Table 1, Supplementary Data). Precision therefore mostly depends on data processing consistency and less on signal strength. In practise this means that as long as H_2O peaks are visible (H_2O signal-to-noise > 2), good precisions can be expected from data processed with silicH$_2$O. Even single analyses likely give results within 2σ of real values are therefore reliable within 0.2 wt.%

While processing the repeat analyses it was apparent that background signals vary in shape and intensity between spectra from single glasses. This means that each spectrum should be processed individually and even analsyses from single samples may need different *BIR* positions. This is important since small changes in *BIR* positions may have significany impact on final calculated H_2O contents. silich$_2$o helps address these issues by providing immediate results and constant visual feedback. Furthermore, *BIR* positions can be easily compared between samples by copying and pasting them between each other (see the documentation[*])

5 SILICH$_2$O HIGHLIGHTS

silicH$_2$O makes post-processing and H_2O quantification of silicate glass Raman spectra straightforward and easily accessible by providing an interactive graphical user interface. Quality control is quick and easy as results and processed spectra are shown in real-time. This results in accuracies and precisions mostly within 0.1 wt.% for H_2O contents quantified with calibrations made within SilicH$_2$O. Interpolation and interference subtraction algorithms for removing unwanted peaks produce results on par with those from samples where no corrections were needed. Overall, SilicH$_2$O provides the tools for consistent processing of Raman spectra in order to produce accurate and precise H_2O quantifications.

AUTHOR CONTRIBUTIONS

T. D. van Gerve did the Raman analyses, conceived the idea of developing stand-alone software, wrote te code and drafted the manuscript. O. Namur conceived the idea of Raman H_2O calibration and contributed to editing the manuscript.

ACKNOWLEDGEMENTS

This work was supported by a FWO (Research Foundation - Flanders) Odysseus grant to O. Namur. We thank Etienne Médard, David Neave and Renat Almeev for providing samples for validation and calibration.

DATA AVAILABILITY

SilicH$_2$O version 1.0.0 can be downloaded as a release from GitHub[†] and detailed installation and usage instructions are available in its documentation[‡]. The software includes the data reported in Section 4 as example projects. If you want to report a bug, request a new feature or contribute to the code, please open an issue or pull request on GitHub. Supplementary texts and data for calibration, validation and precision tests are available in the Zenodo archive at `https://doi.org/10.5281/zenodo.7808302`.

COPYRIGHT NOTICE

REFERENCES

Ardia, P., A. Di Muro, D. Giordano, D. Massare, C. Sanchez-Valle, and M. W. Schmidt (2014). "Densification mechanisms of haplogranite glasses as a function of water content and pressure based on density and Raman data". *Geochimica et Cosmochimica Acta* 138, pages 158–180. DOI: 10.1016/j.gca.2014.03.022.

Behrens, H., J. Roux, D. R. Neuville, and M. Siemann (2006). "Quantification of dissolved H2O in silicate glasses using confocal microRaman spectroscopy". *Chemical Geology* 229(1-3), pages 96–112. DOI: 10.1016/j.chemgeo.2006.01.014.

Di Genova, D., D. Morgavi, K. U. Hess, D. R. Neuville, N. Borovkov, D. Perugini, and D. B. Dingwell (2015). "Approximate chemical analysis of volcanic glasses using Raman spectroscopy". *Journal of Raman Spectroscopy* 46(12), pages 1235–1244. DOI: 10.1002/jrs.4751.

Di Genova, D., S. Sicola, C. Romano, A. Vona, S. Fanara, and L. Spina (2017). "Effect of iron and nanolites on Raman spectra of volcanic glasses: A reassessment of existing strategies to estimate the water content". *Chemical Geology* 475, pages 76–86. DOI: 10.1016/j.chemgeo.2017.10.035.

Di Muro, A., N. Métrich, M. Mercier, D. Giordano, D. Massare, and G. Montagnac (2009). "Micro-Raman determination of iron redox state in dry natural glasses: Application to peralkaline rhyolites and basalts". *Chemical Geology* 259(1-2), pages 78–88. DOI: 10.1016/j.chemgeo.2008.08.013.

Duggen, S., M. Portnyagin, J. Baker, D. Ulfbeck, K. Hoernle, D. Garbe-Schönberg, and N. Grassineau (2007). "Drastic shift in lava geochemistry in the volcanic-front to rear-arc region of the Southern Kamchatkan subduction zone: Evidence for the transition from slab surface dehydration to sediment melting". *Geochimica et Cosmochimica Acta* 71(2), pages 452–480. DOI: 10.1016/j.gca.2006.09.018.

---

[*] https://silich2o.readthedocs.io/en/latest/

[†] https://github.com/TDGerve/silicH2O

[‡] https://silich2o.readthedocs.io/en/latest/

Frezzotti, M. L., F. Tecce, and A. Casagli (2012). “Raman spectroscopy for fluid inclusion analysis”. *Journal of Geochemical Exploration* 112, pages 1–20. DOI: 10.1016/j.gexplo.2011.09.009.

Giordano, D. and J. K. Russell (2018). “Towards a structural model for the viscosity of geological melts”. *Earth and Planetary Science Letters* 501, pages 202–212. DOI: 10.1016/j.epsl.2018.08.031.

Giordano, D., D. González-García, J. K. Russell, S. Raneri, D. Bersani, L. Fornasini, D. Di Genova, S. Ferrando, M. Kaliwoda, P. P. Lottici, M. Smit, and D. B. Dingwell (2020). “A calibrated database of Raman spectra for natural silicate glasses: implications for modelling melt physical properties”. *Journal of Raman Spectroscopy* 51(9), pages 1822–1838. DOI: 10.1002/jrs.5675.

Jochum, K. P., B. Stoll, K. Herwig, M. Willbold, A. W. Hofmiann, M. Amini, S. Aarburg, W. Abouchami, E. Hellebrand, B. Mocek, I. Raczek, A. Stracke, O. Alard, C. Bouman, S. Becker, M. Dücking, H. Brätz, R. Klemd, D. De Bruin, D. Canil, D. Cornell, C. J. De Hoog, C. Dalpé, L. V. Danyushevsky, A. Eisenhauer, Y. Gao, J. E. Snow, N. Groschopf, D. Günther, C. Latkoczy, M. Guillong, E. H. Hauri, H. E. Höfer, Y. Lahaye, K. Horz, D. E. Jacob, S. A. Kasemann, A. J. Kent, T. Ludwig, T. Zack, P. R. Mason, A. Meixner, M. Rosner, K. Misawa, B. P. Nash, J. Pfänder, W. R. Premo, W. D. Sun, M. Tiepolo, R. Vannucci, T. Vennemann, D. Wayne, and J. D. Woodhead (2006). “MPI-DING reference glasses for in situ microanalysis: New reference values for element concentrations and isotope ratios”. *Geochemistry, Geophysics, Geosystems* 7(2). DOI: 10.1029/2005GC001060.

Le Losq, C., D. R. Neuville, R. Moretti, and J. Roux (2012). “Determination of water content in silicate glasses using Raman spectrometry: Implications for the study of explosive volcanism”. *American Mineralogist* 97(5-6), pages 779–790. DOI: 10.2138/am.2012.3831.

Long, D. A. (1977). *Raman Spectroscopy*. New York: MacGraw-Hill, page 267.

Malfait, W. J. (2018). *Vibrational properties of glasses and melts*. Chapter 5. Elsevier Inc., pages 211–236. ISBN: 9780128113011. DOI: 10.1016/B978-0-12-811301-1.00008-3.

McMillan, P. F. (1984). “Structural studies of silicate glasses and melts-applications and limitations of Raman spectroscopy.” *American Mineralogist* 69(7-8), pages 622–644.

McMillan, P. F. and B. Piriou (1982). “The structures and vibrational spectra of crystals and glasses in the silica-alumina system”. *Journal of Non-Crystalline Solids* 53(3), pages 279–298. DOI: 10.1016/0022-3093(82)90086-2.

McMillan, P. F., B. T. Poe, P. H. Gillet, and B. Reynard (1994). “A study of SiO2 glass and supercooled liquid to 1950 K via high-temperature Raman spectroscopy”. *Geochimica et Cosmochimica Acta* 58(17), pages 3653–3664. DOI: 10.1016/0016-7037(94)90156-2.

Médard, E. and T. L. Grove (2008). “The effect of H2O on the olivine liquidus of basaltic melts: Experiments and thermodynamic models”. *Contributions to Mineralogy and Petrology* 155(4), pages 417–432. DOI: 10.1007/s00410-007-0250-4.

Mercier, M., A. Di Muro, D. Giordano, N. Métrich, P. Lesne, M. Pichavant, B. Scaillet, R. Clocchiatti, and G. Montagnac (2009). “Influence of glass polymerisation and oxidation on micro-Raman water analysis in alumino-silicate glasses”. *Geochimica et Cosmochimica Acta* 73(1), pages 197–217. DOI: 10.1016/j.gca.2008.09.030.

Mysen, B. O. (1983). “The structure of silicate melts”. *Ann. Rev. Earth Planet. Sci* 11(1983), pages 75–97. DOI: 10.1090/gsm/146/03.

– (2003). “Physics and chemistry of silicate glasses and melts”. *European Journal of Mineralogy* 15(5), pages 781–802. DOI: 10.1127/0935-1221/2003/0015-0781.

Mysen, B. O. and D. Virgo (1980). “Solubility mechanisms of H2O in silicate melts at high pressures and temperatures : a Raman spectroscopic study”. *American Mineralogist* 65, pages 1176–1184.

Neave, D. A., O. Namur, O. Shorttle, and F. Holtz (2019). “Magmatic evolution biases basaltic records of mantle chemistry towards melts from recycled sources”. *Earth and Planetary Science Letters* 520, pages 199–211. DOI: 10.1016/j.epsl.2019.06.003.

Neuville, D. R., D. de Ligny, and G. S. Henderson (2014). “Advances in Raman spectroscopy applied to earth and material sciences”. *Spectroscopic Methods in Mineralogy and Materials Sciences* 78, pages 509–541. DOI: 10.2138/rmg.2013.78.13.

Neuville, D. R. and B. O. Mysen (1996). “Role of aluminium in the silicate network: In situ, high-temperature study of glasses and melts on the join SiO2-NaAlO2”. *Geochimica et Cosmochimica Acta* 60(10), pages 1727–1737. DOI: 10.1016/0016-7037(96)00049-X.

Pasteris, J. D. and O. Beyssac (2020). “Welcome to Raman spectroscopy: Successes, challenges, and pitfalls”. *Elements* 16(2), pages 87–92. DOI: 10.2138/GSELEMENTS.16.2.87.

Raman, C. V. (1928). “A new radiation”. *Indian journal of Physics*, pages 387–398. DOI: 10.1007/BF03052651.

Schiavi, F., N. Bolfan-Casanova, A. C. Withers, E. Médard, M. Laumonier, D. Laporte, T. Flaherty, and A. Gómez-Ulla (2018). “Water quantification in silicate glasses by Raman spectroscopy: Correcting for the effects of confocality, density and ferric iron”. *Chemical Geology* 483, pages 312–331. DOI: 10.1016/j.chemgeo.2018.02.036.

Sharma, S. K., J. F. Mammone, and M. F. Nicol (1981). "Raman investigation of ring configurations in vitreous silica". *Nature* 292(5819), pages 140–141. DOI: 10.1038/292140a0.

Shishkina, T. A., R. E. Botcharnikov, F. Holtz, R. R. Almeev, and M. V. Portnyagin (2010). "Solubility of H2O- and CO2-bearing fluids in tholeiitic basalts at pressures up to 500MPa". *Chemical Geology* 277(1-2), pages 115–125. DOI: 10.1016/j.chemgeo.2010.07.014.

Thomas, R., N. Metrich, B. Scaillet, V. Kamenetsky, and P. Davidson (2008). "Determination of water in Fe-rich basalt glasses with confocal micro-Raman spectroscopy". *Z. Geol. Wiss* 36(1-2), pages 31–37.

Umari, P., X. Gonze, and A. Pasquarello (2003). "Concentration of Small Ring Structures in Vitreous Silica from a First-Principles Analysis of the Raman Spectrum". *Physical Review Letters* 90(2), page 4. DOI: 10.1103/PhysRevLett.90.027401.

van Gerve, T. D., D. A. Neave, P. Wieser, H. Lamadrid, N. Hulsbosch, and O. Namur (2023). "Lower crustal magma storage and differentiation in Ocean Island volcanoes: Integrating 3D imaging with chemical microanalysis of olivine-hosted melt inclusions from Pico (Azores)". *Journal of Petrology (under review)*.

Zajacz, Z., W. Halter, W. J. Malfait, O. Bachmann, R. J. Bodnar, M. M. Hirschmann, C. W. Mandeville, Y. Morizet, O. Müntener, P. Ulmer, and J. D. Webster (2005). "A composition-independent quantitative determination of the water content in silicate glasses and silicate melt inclusions by confocal Raman spectroscopy". *Contributions to Mineralogy and Petrology* 150(6), pages 631–642. DOI: 10.1007/s00410-005-0040-9.